CAAP Quarterly Report

Date of Report: *July 9, 2015*

Contract Number: *DTPH5614HCAP04*

Prepared for: *Dr. James Merritt, PHMSA-DOT*

Project Title: *Optimized Diagnosis and Prognosis for Impingement Failure of PA and PE Piping Materials*

Prepared by: *University of Colorado-Denver, Arizona State University*

Contact Information: *Dr. Yiming Deng and Dr. Yongming Liu*

For quarterly period ending: *July 10, 2015*

Business and Activity Section

(a) Generated Commitments

Pipeline infrastructure and its safety is critical for the recovering of U.S. economy and our standard of living. Statistics from U.S. Department of Transportation (DOT) and Gas Technology Institute (GTI) show the decline in use of steel and cast iron piping materials is significant in recent years and the increase in pipeline system size is largely due to plastic pipe installations. However, failure inevitably occurs in plastic piping materials and impingement failure is caused by high localized stress concentration combined with defects and inclusions. Previous research efforts were mainly focusing on PE materials, efficient and effective impingement damage diagnosis and prognosis of various types of new plastic piping materials still remain unaddressed and challenging. The proposed research will fundamentally understand and characterize the failure modes and associated material behaviors for modern plastic piping materials. The proposed optimized diagnosis and prognosis approaches will thoroughly investigate and compare the dominating PE materials (make up nearly 97% of current plastic pipes) and the emerging PA pipes that can operate at much higher pressures and be installed using existing PE tools and techniques. If successful, this study can help to effectively maintain and improve the reliability of pipeline systems, and ultimately reduce the environmental consequences because of a pipeline catastrophic failure.

The overall objectives of the proposed research are two-fold: optimized diagnosis-find existing impingement damage at the earliest stage before it becomes failure critical in PE and PA materials, conduct comprehensive comparison studies to identify the differences in micro-cracking mechanism between these two materials; and optimized prognosis - accurately predict the remaining strength and RUL of PE and PA components through mechanical modeling and experimental investigations.

The eighteen-month effort will establish a framework composed of both physical (CU) and mechanical modeling (ASU) with optimized parametric studies both numerically and experimentally, and models validation during the first project year (month 1 to month 12). A thorough anomaly detection, characterization and sensitivity analysis for both optimized diagnosis and prognosis algorithms will be carried out in the second project year (month 13 to month 16). Building upon achieving these research milestones, a model-assisted detection and prediction framework with the integrated diagnosis and prognosis capabilities will be realized and tested in field at the last phase of this project (month 16 to month 18). The specific technical objectives are addressed through the

following two major research tasks, each has three subtasks:

Task 1 focuses on the sensing physics modeling of impingement failure diagnosis and experimental investigation assisted by model-based inversion techniques. Three subtasks are proposed: (1.1) element-free Galerkin's method (EFG) development for the electromagnetic modeling of arbitrary and micro-scale crack initiation and propagation due to impingement; (1.2) model-based inversion for ultra-fast impingement failure reconstruction and sensing assisted by compressed sensing techniques; (1.3) demonstration of optimized diagnosis capabilities using electromagnetic diffraction tomography array.

Task 2 focuses on the mechanical modeling of impingement failure and experimental investigation. Three subtasks are proposed: (2.1) extended finite element method (XFEM) and cohesive zone modeling (CZM) for the crack initiation and propagation simulation; (2.2) experimental investigation of impingement effect on the failure of investigated materials; (2.3) parametric study and sensitivity analysis for the optimized prognosis algorithms.

(b) Status Update of Past Quarter Activities

Task 1- Sensing physics modeling of impingement failure diagnosis and experimental investigation assisted by model-based inversion techniques for PE and PA meterial

Subtask 1.1 Physics modeling for imaging of PE and PA piping materials

Polyethylene(PE) is a cost effective solution for a broad range of piping problem in a variety of industries. It has been tested and proven effective for above ground, surface, buried applications. High-density polyethylene pipe (HDPE) can carry portable water, wastewater, chemicals, and compressed gases. Polyethylene is strong, extremely tough and very durable. Since it is a plastic material, polyethylene does not rust, rot or corrode, this will lower the life cycle costs.

PA11 is a material of choice for corrosion free, aggressive hydrocarbon transport system. PA11 thermoplastic material has been used across the entire oil and gas value chain extensively, for cost-effective non-metallic piping systems. PA11 provide a better value compare to steel pipe. It has lower total installation cost, lower lifetime maintenance, and comparable performance. According to a brochure from ARKEMA, PA11 also shows excellent resistance to slow crack growth.

Simulation study is an important way to assist experimental studies and sensor development via optimization of critical parameters. In this quarter, we developed a FEKO model to assist the experiment scanning. The goal of the simulation is to study the electric field distribution along the target to verify the experiment results. The scanning probe is designed as a monopole antenna in the simulation which is mounted on an infinite perfectly electric conducting ground. We chose infinite PEC ground to avoid the reflection due to the size of ground plane. The cutoff frequency of the probe tip set at 3GHz, the size of the monopole antenna is quarter of wavelength, which is 2.5cm. First, we design a PA material with size of 13.375in x 19.125in x 0.313in, a hole with a radius of 5mm is introduced at the center of the target. Since the size of the probe tip is 2mm, this will help us identify the resolution of the scanning probe. Fig 1(a) below shows the design of the simulation. We move probe tip along x direction to see if the probe tip is able to detect the whole at the center.

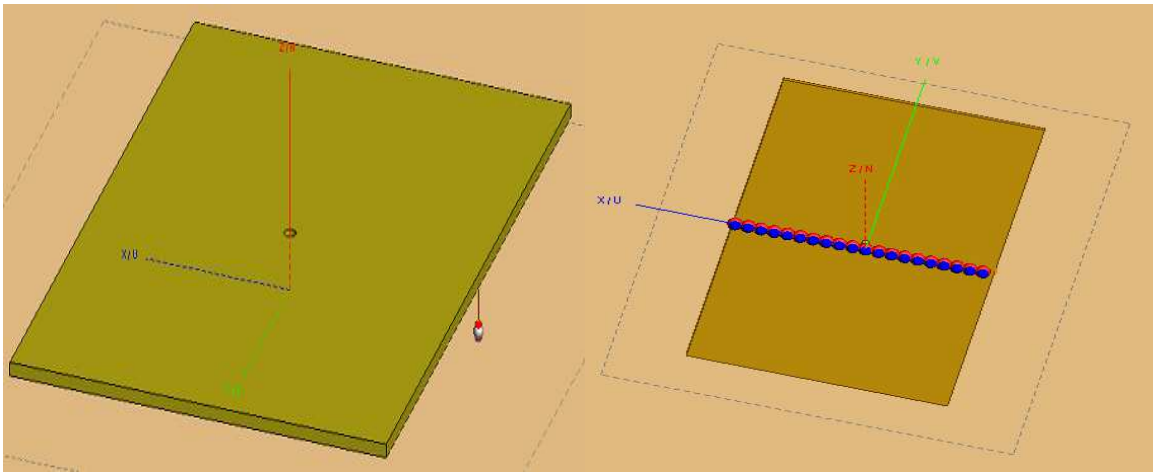

(a) (b)

Fig. 1 Simulation geometry of the PA material

Due to the processing speed of the computer, we put 20 probe tip along x direction at the center of the sample as shown in Fig. 1(b). This will reduce the simulation time. Fig.2 shows the simulation result along both x and y direction. From Fig. 2 we can clear see that there is a whole right at the center of the target from both x and y direction. The ripples that show in the results are due to the radiation between each scanning probe tip. The distance between each probe tip is 17mm, which is less than one wavelength, this will introduce noise to the results. Even with the noise we have, we can still clear see the hole from the center, this gave us the confident that the size of the probe tip is good enough to achieve high resolution images.

Next, we design a simulation for PE material. The size of the sample is 18in x 12in x 0.4in. Several defects have been introduced to the sample as the experiment setup to verify the experiment results. As shown in Fig. 3, we introduced different sizes of square to the sample. The depth of the square is 0.236in, which is thinner than the sample. The length of the sides of each square is 3in, 2in, 1.5in and 1in. We locate the probe tip on the smooth side of the sample, to see if we are able to detect the defects. We move probe tip only along y-axis, the simulation results should be able to show the different size of squares.

Fig. 4 shows the result of the PE material simulation. From the results we can clear see the four squares along y-axis. Since we put the probe tip at the smooth side, this proof the capability of the probe tip for penetrating the material and also able to detect the defect. The ripples in the Fig.4(b) also caused by the close distance between each probe tip. To improve the simulation design and also develop the algorithm for meshless model will implement during the next quarter.

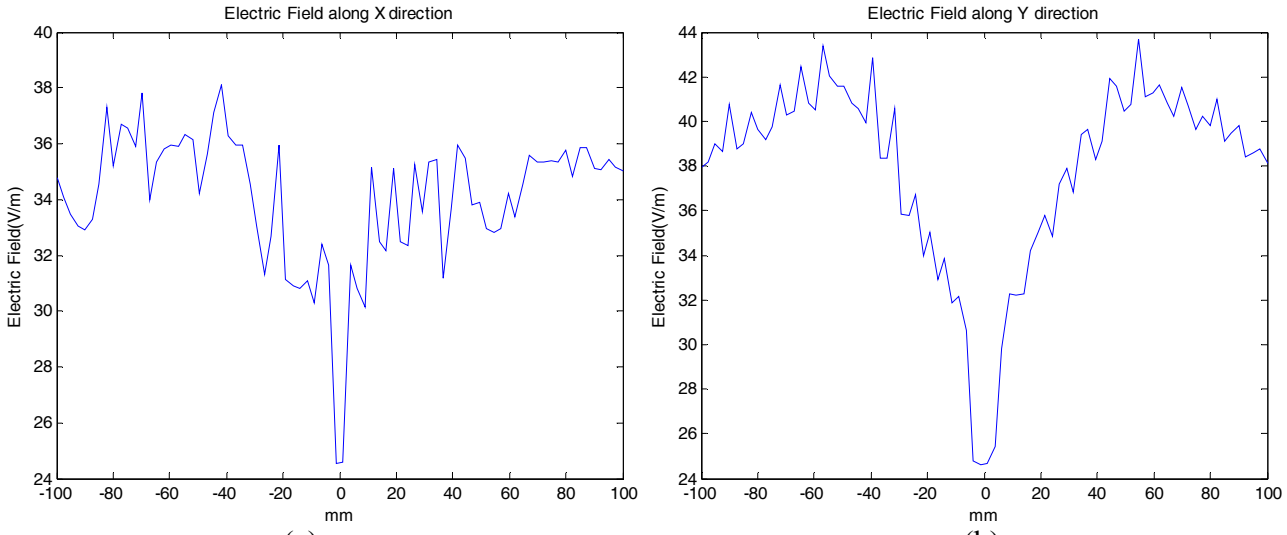

(a) (b)

Fig. 2 (a) Electric field achieved from X direction. (b) Electric field achieved from Y direction

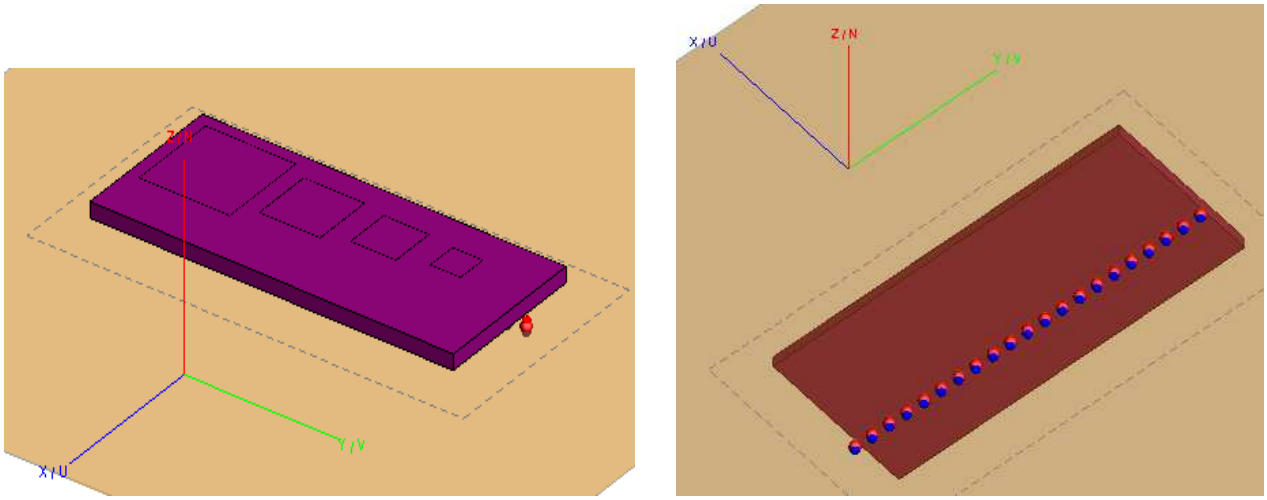

Fig. 3 Simulation geometry of the PA material

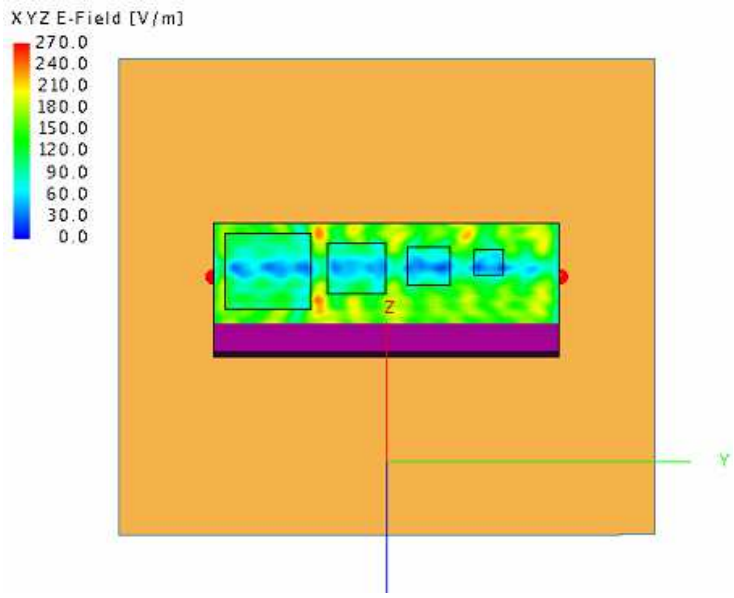

(a)

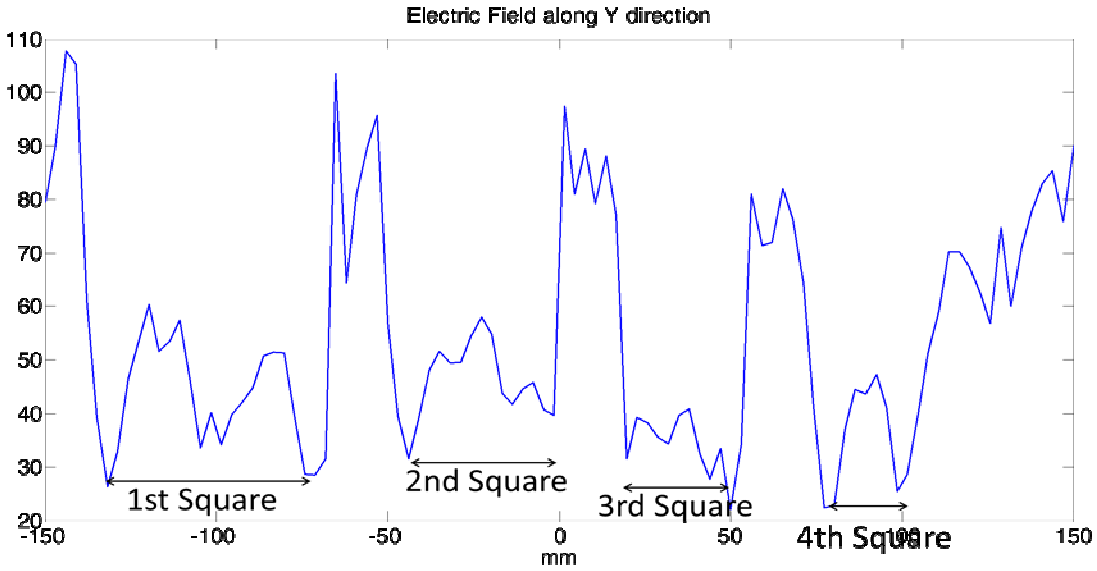

(b)

Fig. 4 Simulation results for PE material

In the meantime, CU LEAP team is developing the EFG solver for better PE and PA damage imaging capability. The progress of this subtask is presented below:

Element-free Galerkin Method

Finite element method is a very general and powerful numerical method for solving the boundary value problem. One drawback of this method is the heavy workload of the data preparation which due to the meshing calculation, especially for the complicated three-dimensional problem. When simulating plastic materials which might have crack propagation or large deformations, it would be hard to maintain the connectivity of the mesh and result in error output. Therefore, remeshing is usually needed and leading to high computational cost. Many difficulties associated with Finite element method have been solved by the element-free Galerkin (EFG) method. As a new type of numerical methods, meshless method is no longer depending on the concept of element. This type of methods avoid the heavy workload of mesh generation and element distortion.

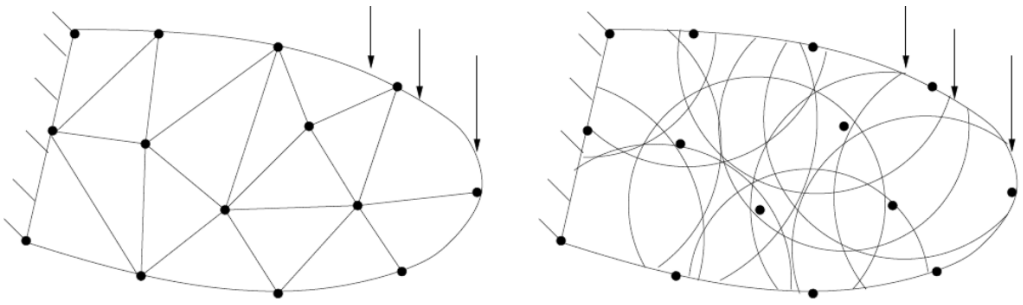

Finite element method Element-free Galerkin method

Fig.5 Nodes in mesh and meshless method

Moving Least Square Method:

Moving least square is a meshless way to approximate functions. If the Approximate expression of an Unknown field function $u^h(x)$ can be Simulate as:

$$u^h(x) = \sum_{j=1}^{m} p_j(x) a_j \equiv P^T(x) a(x)$$

Where m represent the dimension of basis function. P(x) is the polynomial basis vector.

$$P(x) = [p_1(x), ..., P_j(x) ..., p_m(x)]^T$$

For Two dimensional linear basis: $P(x) = [1, x, y]^T$

For Two dimensional quadratic linear basis: $P(x) = [1, x, y, x^2, xy, y^2]^T$

a(x) is the Global coefficient vector, which is:

$\mathrm{a}(\mathrm{x}) = [\mathrm{a}_1(x), a_2(x), ...a_m(x)]^T$

In order to solve the value of a(x), MLS try to find the minimum value of:

$$J(x) = \sum_{I=1}^{N} W(x - x_1)[P^T(x_I) a(x) - u_I]^2$$

W(x) is the weight function. The weight function has a great influence on the result of least squares fitting. Selection generally follows the following rules:

(1) The weight function remains non negative under any circumstances;

(2) The weight function of compact support domain should ensure the existence and uniqueness of A - 1 (x);

(3) The points at the different distance to the fitting point have different influence.

Accuracy analysis of the Moving Least Square Method:

When using moving least square method to find the function approximation by establishing the shape function and solve the numerical solution for partial differential equations. The reasonable establishment of the shape function directly determines the accuracy of function approximation and numerical results.

The rational establishment of the shape function is determined by the following three aspects:

(1) the selection of weight function
(2) the order of basis functions;
(3) domain of influence of each node

In order to study the influence of the order of the basis functions and the influence of nodes on the function approximation and the numerical solution precision. Gauss weight function is selected as the weight function. Several pairs of basis functions and node's domain of influence have been evaluate in order to find the general rule of the reasonable establishment of the shape function. The approximation function is f(x) = x*sin(x) with length 10.

Figures below are the comparisons between the approximation function and the reference function. In each figure, the original function, the first order derivative and the second order derivative are shown from top to bottom, respectively. The blue line is the reference function, and the red line is the approximation function.

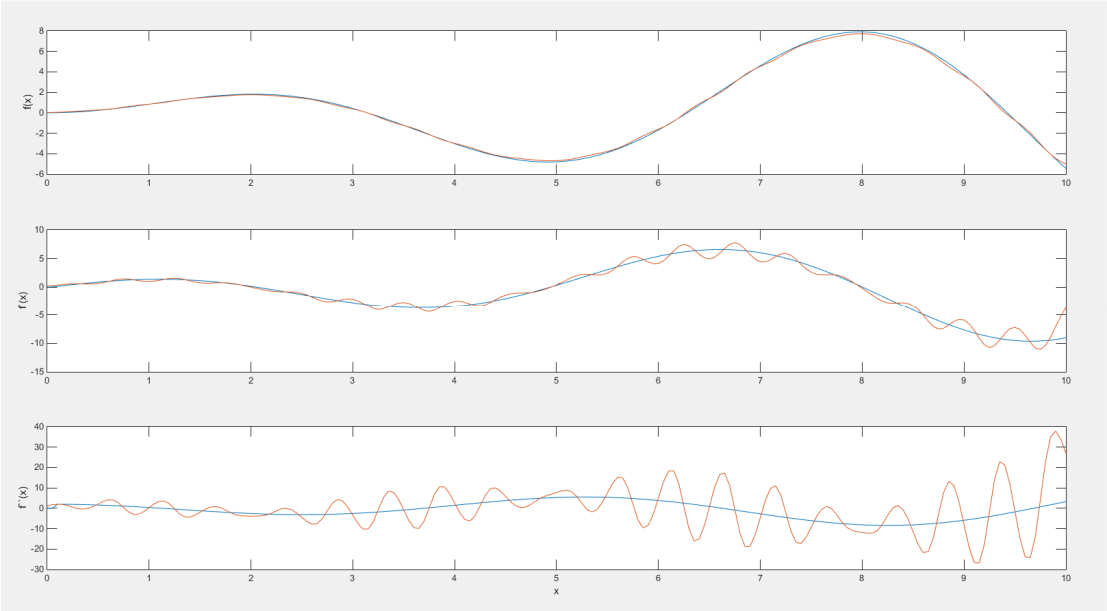

Fig.6 Constant basis with nodes' Radius of support equal to 2

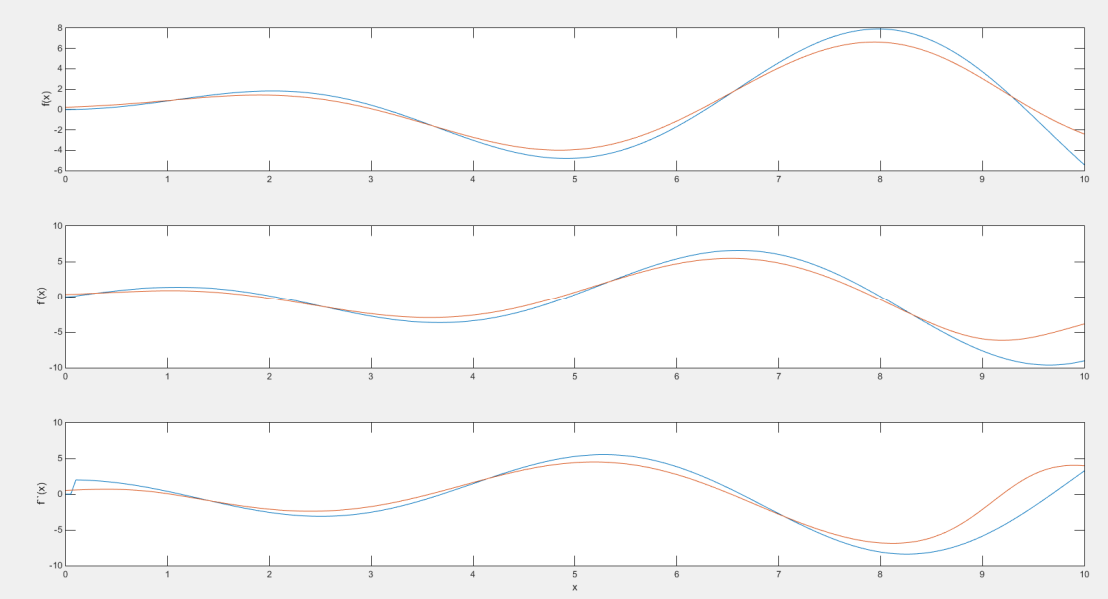

Fig.7 Constant basis with nodes' Radius of support equal to 5

As figures shown above, for a constant basis function, the errors of fitting function and the derivative of each order is large with a small influence domain of each node. The numerical oscillations disappear when the domain of influence of nodes are increased. However, the approximation results still have large errors. This might due to the constant basis function gives low order shape function, which resulting in a big approximation error of higher order function simulation.

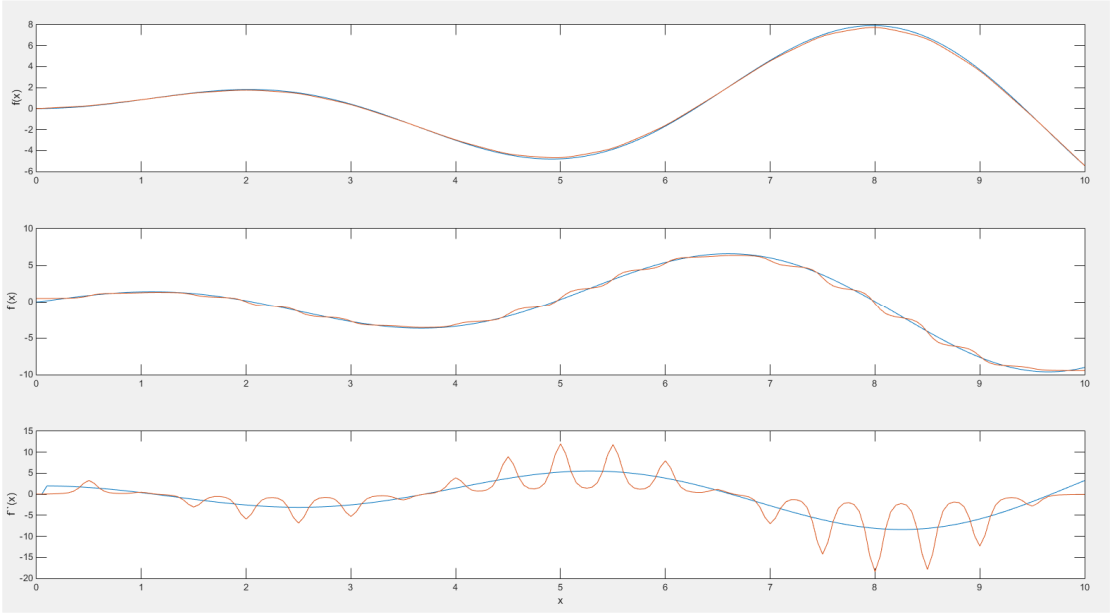

Fig.8 Linear basis with nodes' Radius of support equal to 2

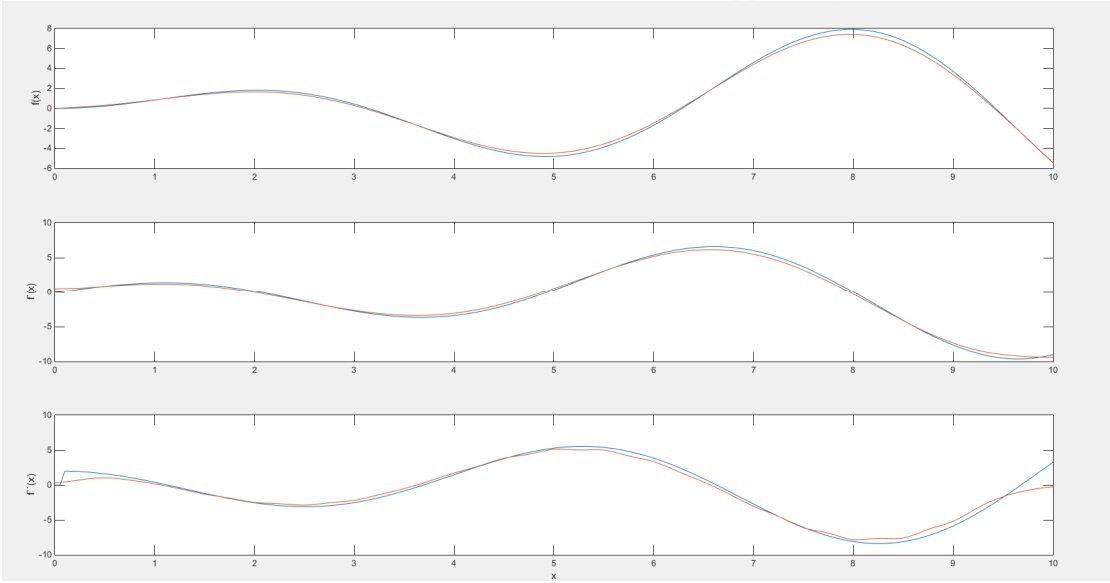

Fig.9 Linear basis with nodes' Radius of support equal to 5

As figure shown above, a better performance is given when applying the linear basis function. Approximation function can obtain better accuracy as the domain of influence of nodes increase. Figure below shows that quadratic basis function resulting in a huge error with low nodes' support radius. Numerical oscillations vanish when approaching a higher nodes' support radius, the error of first derivative and the second derivative is still larger than the result of linear basis function.

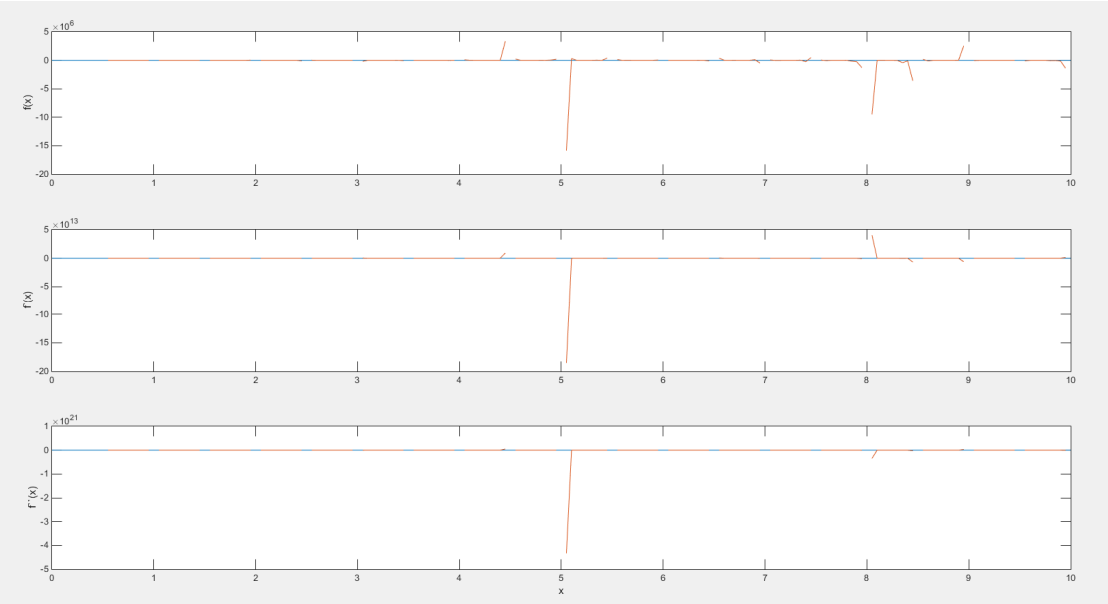

Fig.10 Quadratic basis with nodes' Radius of support equal to 2

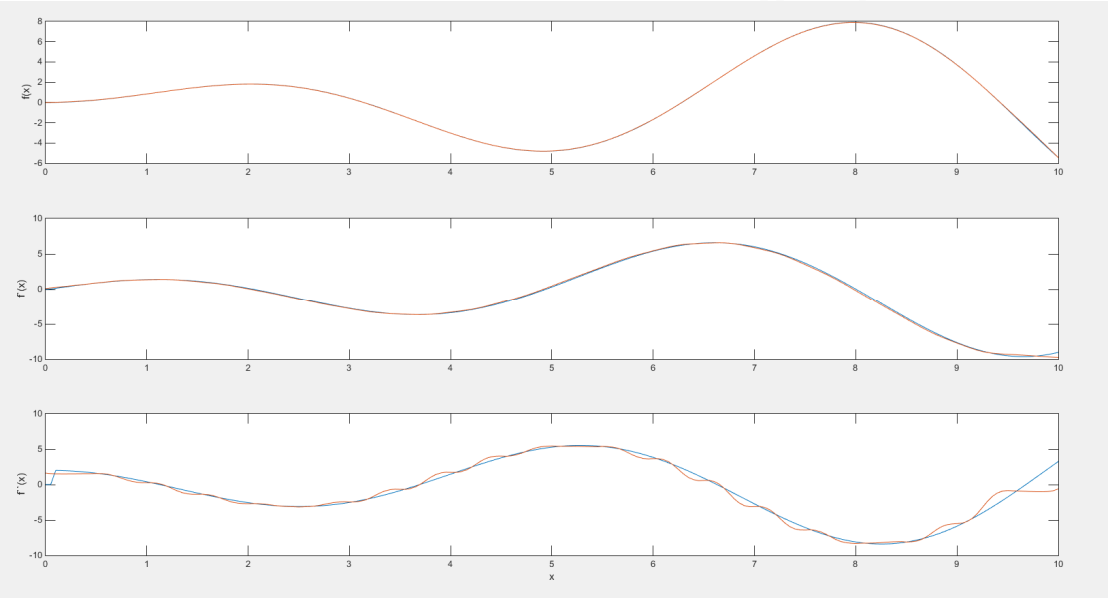

Fig.11 Quadratic basis with nodes' Radius of support equal to 5

Therefore, the approximation accuracy can be determined by using the appropriate basis functions and the number of fitting nodes within the influence region. Using the high order polynomial function as the basis function to construct the shape function, it may lead to numerical oscillation instead of improve the accuracy.

Subtask 1.2 Experimental measurements and sensing development

Measuring the amplitude, or the intensity, of the reflected signal is one of the important parameters which one can measure. The localized reflected microwave amplitude carries information about the complex dielectric constant of the material. Using a sharp antenna tip results to acquiring data with high special resolution. In our experiment the probe, in many cases a coaxial tip antenna CTA, is brought within close proximity of the sample surface, and the sample is illuminated with microwaves at 7 GHz. The microwaves experience changes relative to the incident waves. Changes are tightly related to the dielectric properties of the PA and PE sample. It should be noted that the resolution is directly related to the tip geometry. Using sharper tips result to confining sample interaction area which lead to a better resolution.

We used the raster scan technique to scan the sample and reconstruct the 2D images which are shown in the result part. The experiment set up is shown in Fig. 12.

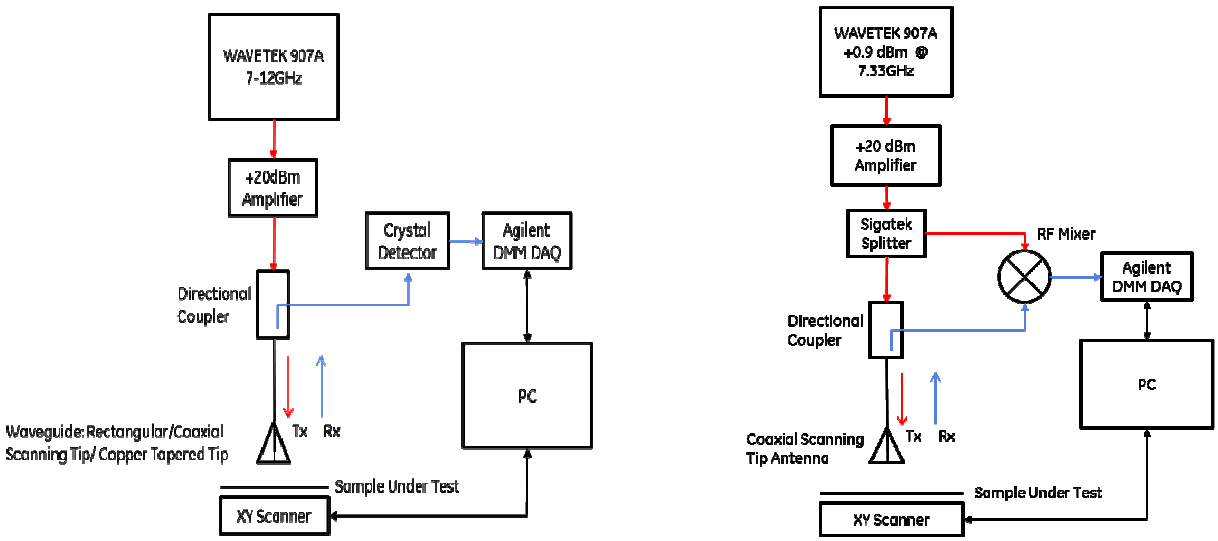

Amplitude Detection Setup Phase Detection Setup

Fig. 12 Amplitude and Phase Detection Setups.

Preliminary Results

The images obtained from PA and PE samples successfully demonstrated the use of microwaves in the near-field range for damage detection for piping materials. The resolution of these images depends on the shape and size of probe tip and the distance between probe tip and target. Current Research is focused on using Co-axial cable antenna which has been initially demonstrated that it can obtain better scanning results comparing to other probe types like open ended waveguide. But the inner conductor of the co-axial cable is not mechanically solid enough to perform any contact scan, which we believe can improve the resolutions further and acquire surface topology as well. The PA and PE samples were scanned at 7GHz as the defects were hidden beneath the sample as shown in the following figures.

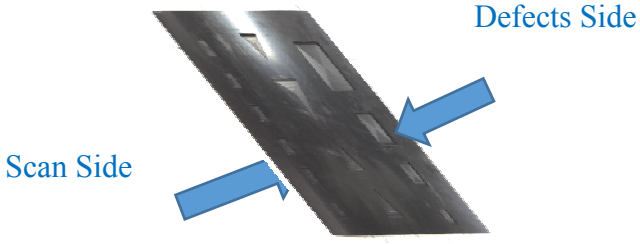

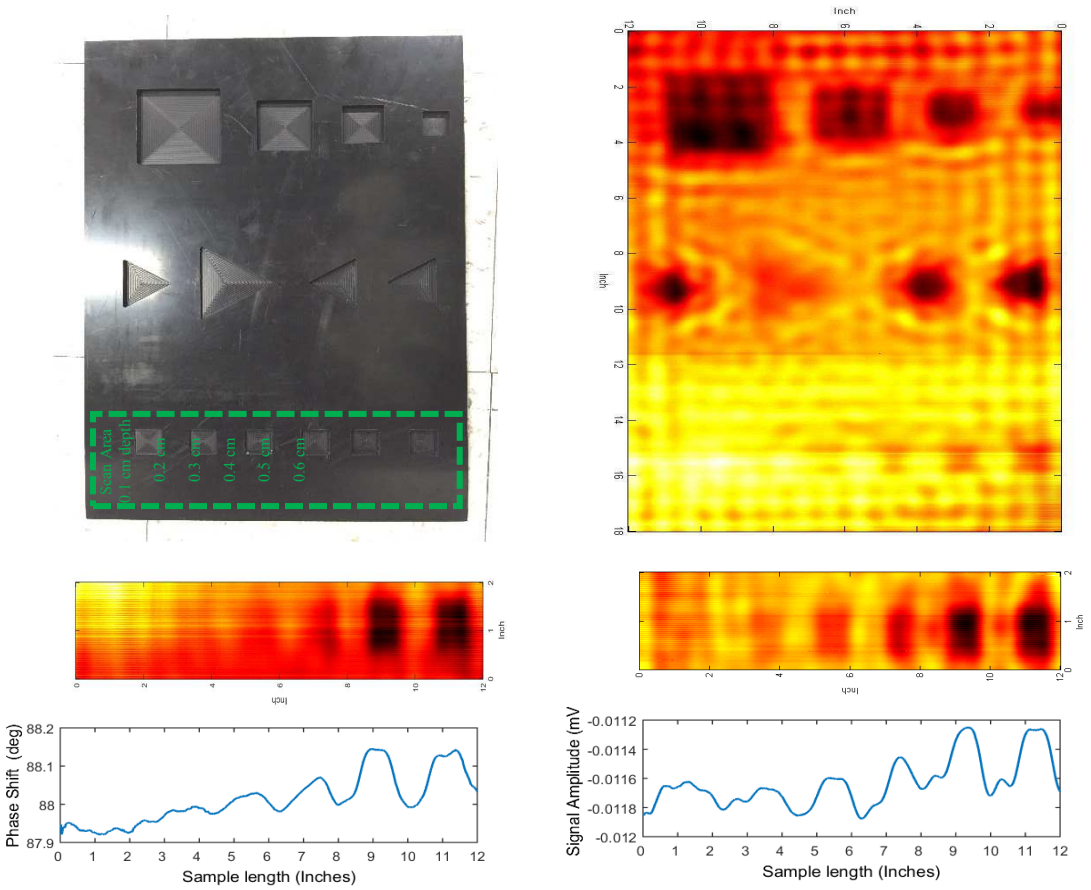

Phase measurement Amplitude measurement

Fig. 13 Polyamide (PA) sample reconstructed images.

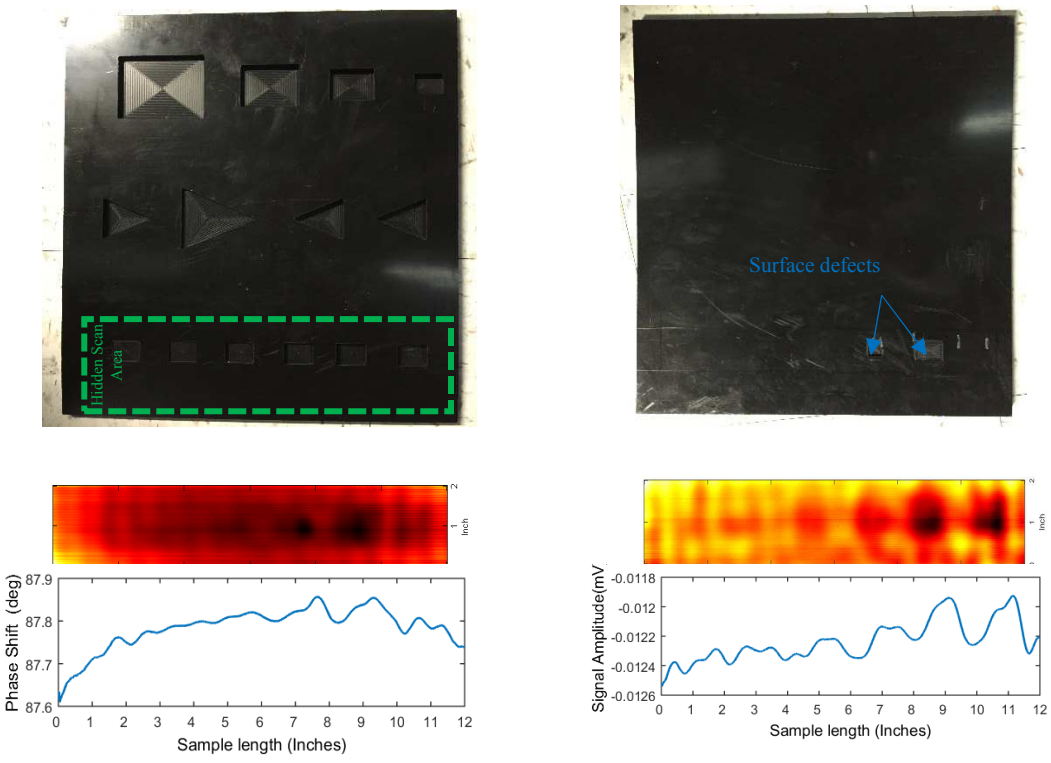

Phase measurement Amplitude measurement

Fig. 14 Polythene (PE) sample reconstructed images.

Near field microwave imaging is far better resolution than the far filed. Amplitude and phase information were retrieved with high special resolution. Phase information extraction using frequency mixing is inexpensive, easy to implement approach. Using RF Siga Tek SM1717. This approach was capable to extract phase information of the scanned sample to construct 2D images that represent variation in the sample properties. Primary high resolution Images were abstained and presented in this report. Different damage signal signatures were observed for PA and PE samples. Raw data will be provided to ASU team for further probabilistic analysis. Currently, LEAP team is also pursuing to improve scan efficiency. The team is working to utilize fast imaging capability using sparse signal reconstruction, e.g. compressed sensing based approach to improve scan timing as well as image resolution. A multichannel model is been developed where the antenna array is configured with different geometries. A 3D simulation study for the cylindrical array was simultaneously conducted using FEKO software.

Task 2-Mechanical modeling on impingement failure

Task 2 focuses on the mechanical modeling and comparison of PA and PE materials. Two major subtasks are performed: 1) preliminary development of a coupled diffusion fracture simulation framework to consider the effect of hydrogen diffusion on the mechanical performance of PE and PA materials; 2) experimental testing fir the investigation of impingement effect on the material failure strength and strain. In this quarterly report, results of subtask are summarized and discussed. Preliminary development of the modeling effort is ongoing and will be presented in the Q4 report.

Subtasks 2.2 Experimental investigation of impingement effect on material strength

2.1 OBJECTIVE

The major research objectives of the project are:

- Simulate the pipe crack propagation using XFEM and investigate the effect material properties, pressure, and crack geometries to the final failure.
- Design of experiments and response surface method to construct a function between the load carrying capacity with respect to design variables.
- Perform probabilistic reliability analysis considering the uncertainties

In the last quarter report, a methodology was defined on how to simulate Slow Crack Growth under creep behavior with given loading conditions. The investigation focused on the time dependent failure of pipeline structures. As done earlier in all simulations, XFEM and cohesive zone model were also used. The challenge in this kind of simulation was to achieve coupled behavior that being cracks initiation and propagation dominated by creep model. This methodology was adopted for two kinds of universal specimens and then were later incorporated into the pipe model.

This particular report encompasses the methodology and outcomes of the short term tensile testing of Polyamide 11 (PA 11) samples along with its strain maps obtained using Digital Image Correlation (DIC) technique. This investigation focuses on experimentally obtaining the mechanical properties of PA 11 and thus tune the parameters that were used to build the XFEM and Cohesive Zone models to match the experimental data. In addition to this, PA 11 samples with a hole of varying depths at its center are also tested in order to simulate impingement effects experimentally and this data will also be used to match with numerical simulation on ABAQUS (in progress).

2.2 INTRODUCTION

The testing of plastics includes wide variety of thermal, chemical and mechanical tests. This particular article reviews the standardized tensile testing method i.e. ASTM D638 along with the various practices adopted by engineers and scientists to test for the tensile properties of plastics. Tensile test embraces

various procedures by which modulus, strength and ductility can be assessed. Generally, the term 'tensile test" means a test wherein a slender specimen is extended uniaxial at a uniform rate. Ideally, specimen should be slender with constant cross section across the gage length, free to contract laterally and expand longitudinally. Though this test was initially designed for testing metals, it was later adopted and adapted for testing plastics and polymers. In the case of plastics, the adaptation had to encompass for the visco-elastic behavior, probable anisotropy of the product. The deformation mechanism of polymers differs from that of metals. In most polymers, only about half of the work of plastic deformation is liberated as heat.

In case of metals, the plastic deformation results in relative change of orientations and positions of metal molecules. So, the large amount of stored integral energy of the polymers have many effects not seen in case of metals. One consequence is, when a unconstrained polymer that has undergone plastic deformation is heated, it will contract toward its original length [1]. The ultimate tensile strength of most of the plastics ranges from 50-80Mpa. The mechanical behavior of polymers is a function of temperature as well as time. So, the data based on short term test have possibility of misinterpreting the results of tested polymers in a design application involving long-term loading conditions.

2.3 FACTORS AFFECTING TESNISLE TEST DATA

Plastics are visco-elastic materials, in which deformation can be dependent on temperature as well as time. Probable anisotropy in the plastic can affect the tests [2].

Viscoelasticity: The time dependence of the deformation of visco-elastic materials can be attributed to rate at which stress is applied. The temperature dependence will depend on the properties of plastic itself which are different for amorphous, crystalline and semi-crystalline [3][4]. As a result, during the tensile test the specimen may distort near grips and clamping forces may relax with passage of time. The subsequent force displacement curves obtained from the tests performed would have time dependence as well as effect of strain rate incorporated [2]. To this effect, Reis et al proposed a model and validated them to evaluate mechanical tensile properties at different strain rates for HDPE [5]. Serban et al reported that for semi crystalline polymers temperature & strain rate changes affects Young's modulus the most with minimal impact on tensile strength [6].

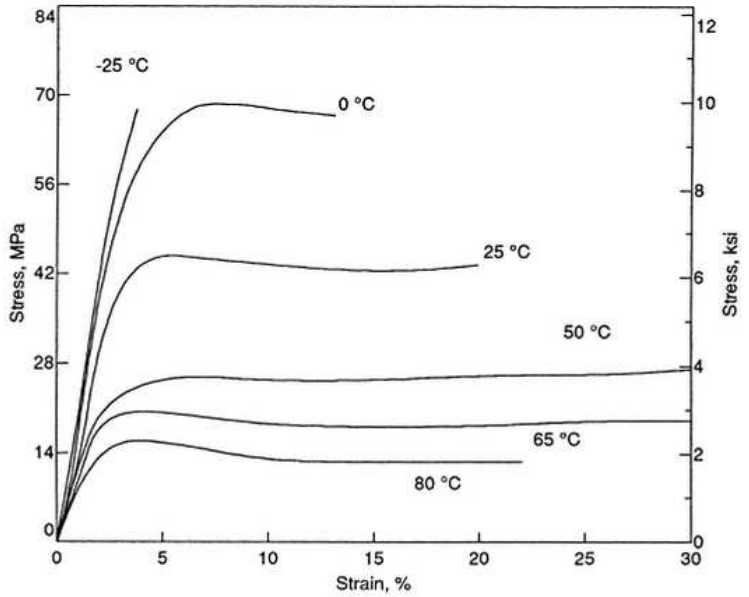

Fig. 15 Influence of Temperature on Stress- Strain curves, Stain rates have a similar effect [2]

Anisotropy: Due to anisotropic behavior of certain plastics, the specimens under investigation have a tendency to deform in irregular ways and may break at points other than those which have minimum cross-section. There are chances that failure takes place at the grips unless special precautions are taken. So, as a result of which the moduli and strength may be higher or lower than expected due to this anisotropy that may be introduced by flow geometry [7]. Recent work on this by Dyamenahalli0 et al in

the characterization of shape memory polymers for tensile properties conclude that for anisotropic polymers which have discontinuous phase requires use of biaxial testing systems [8].

3.0 UNIAXIAL TENILE TEST ASTM D638

ASTM D638 is one of the more popular mechanical tests of plastics employed to determine tensile properties of unreinforced and reinforced plastics [9] under specified shape, condition of pre-treatment, temperature, humidity and testing machine speed. This test is designed to produce tensile property data for control & specifications of plastic materials. Important parameters from this test include ultimate tensile test (UTS), Young's stress, Poisson's Ratio, elongation at yield [8]. Data from this test has been found useful in engineering design with a precaution that data cannot be exactly used for design calculations if the environment of use is different from that of testing.

Recent works on polymer tensile testing conducted in controlled environment include:

- El Mourid et al – performed D638 tensile tests on aged polymer matrix composites at maximum service temperature to evaluate degradation of polymer matrix and performed tests in two different directions to explore anisotropy of the material [10].
- Sadeghian et al – performed D638 tensile testing on welded Acrylonitrile butadiene styrene (ABS) sheets. In order to avoid defects in the weld joint, samples were prepared from core of weld joints [11].
- Castagnet et al – performed tensile test on PA-11 and PE samples in hydrogen, nitrogen and air environment to determine the effects on mechanical properties [12].

Specimen Preparation: One of the important parts of D638 is specimen preparation. Care should be taken to ensure all samples are prepared in exactly the same way. Because mechanical properties are sensitive to temperature and absorbed moisture, conditioning procedure for test specimen have been developed and defined in ASTM D618 & ISO 291. ASTM D638 has laid down specimen drawings with five types of dimensions depending on the desired thickness and testing conditions.

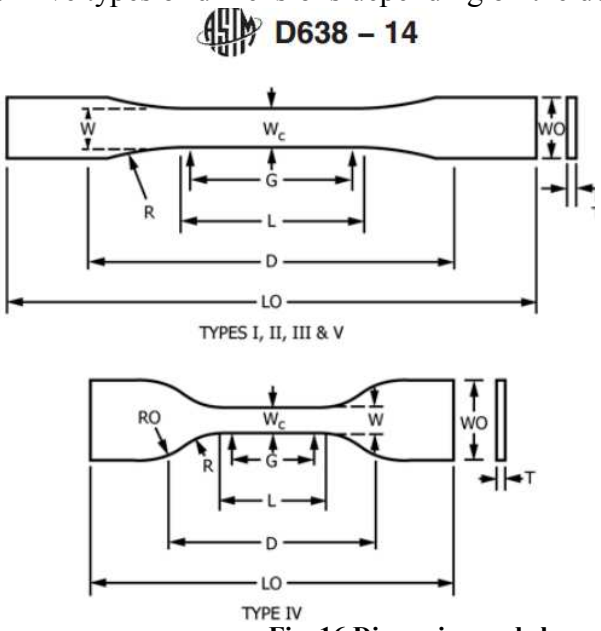

Dimensions (see drawings)	Type I
W—Width of narrow section[E,F]	13 (0.50)
L—Length of narrow section	57 (2.25)
WO—Width overall, min[G]	19 (0.75)
WO—Width overall, min[G]	...
LO—Length overall, min[H]	165 (6.5)
G—Gage length[I]	50 (2.00)
G—Gage length[I]	...
D—Distance between grips	115 (4.5)
R—Radius of fillet	76 (3.00)
RO—Outer radius (Type IV)	...

Fig. 16 Dimension and shape Type 1 specimen from ASTM [20]

Some of the recent works on specimen preparation for polymer tensile testing include:

- Kaymacki el al prepared specimen according to standards by Injection molding process [13].
- El Mourid et al prepared samples by water jet cut adhering to standards [10].
- Negi et al prepared polyamide samples by process optimized Selective Laser Sintering Process (SLS) for tensile test [14].
- Torrodo et al 3D printed specimen by Fused Deposition Modelling (FDM) in both vertical and horizontal orientation to analyse strength in both orientation [15].

- Salazar et al prepared PA11 and PA12 samples by SLS [16]. Recent works on ASTM D638 tensile testing include:
- Kashfuddoja et al used Digital Image correlation (DIC) to obtain stress-strain curves and reported them to be in close agreement with extensometer results [17].
- George et al by ASTM D638 determined the work of failure (WOF) and also quantified the brittleness of HDPE polymer [18] .
- Knorr et al used D638 for cross-linked polymers to ascertain quasi static mechanical properties and used DIC to determine strain rates [19]

4.0 EXPERIMENTAL PROCEDURE

4.1 Test specimen preparation.

Test specimens of ASTM Type 1 were used in the short term tensile testing. The material used for the testing is Polyamide 11. In order to introduce an impingement, holes were drilled at the mid-section of the specimen. The circular holes, which were of varying size and depth, were drilled by the NC Machining center as shown in Fig. 16. The maximum and minimum diameter of the hole were ¼'' & 1/8'' respectively. With regards to depth of the hole, it was either a through hole or a hole that was as deep as half of the specimen's thickness. Speckle pattern were created on each of the specimens for DIC strain measurements.

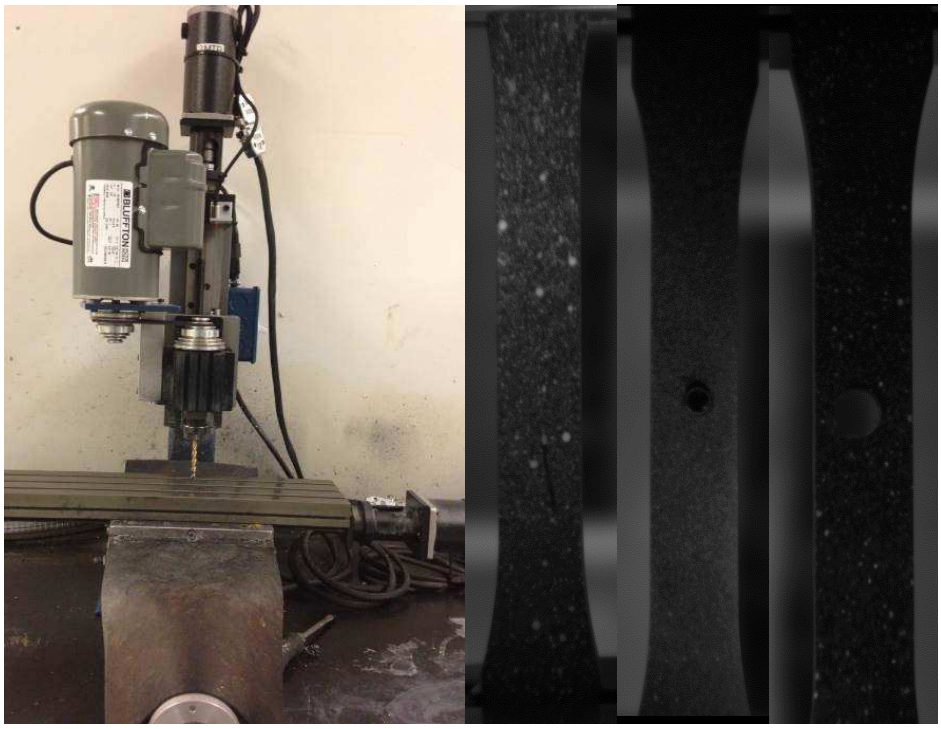

Fig. 17 NC Drilling Machine and specimens with and without holes of varying size and depth.

4.2. Measurements

Tensile tests were performed on a universal testing machine (make; MTS Alliance 10/R) as presented in Fig. 17. The ultimate tensile strength, % elongation, yield strength (at 0.2% strain), and Young's modulus of each of the specimens at 0.2 in/min strain rate and 2'' gauge length was measured for each specimen. Strain measurements of each of the specimens tested were accomplished by optical technique, namely Digital Image Correlation (DIC). Images were captured using Lumenera Infinity 2 Camera. The captured images were analysed by commercial DIC tool called Vic-2D.

Fig. 18 MTS Universal Testing Machine along with camera

4.3 Design of Experiments:

The DOE involved selecting parameters that would affect the mechanical property of PA11 and demonstrate the effects of impingement on the material. The variable parameters that were considered are size (diameter) and depth of the hole. The response parameters were Ultimate load, % elongation. Test matrix was prepared accordingly as shown in Table 1.

Specimen No.	Run order	Depth of impingement [a]	Diameter of impingement
N1	3	0	0
N2	7	0.12''	¼''
N3	6	0.12"	1/8''
N4	1	0.06"	¼''
N5	5	0.06"	1/8"
N6	4	0.06"	1/8"
N7	2	0.06"	1/8"

[a] Avg. thickness of specimen 0.12"

Table 1. Tensile test matrix

5.0 RESULTS AND DISCUSSION

A total of 7 experiments were conducted at two independent input variables as per designed plan. Experimental design matrix with measured data is presented in Table 1. The images were captured for optical strain measurements. DIC analysis was executed using Vic-2D software

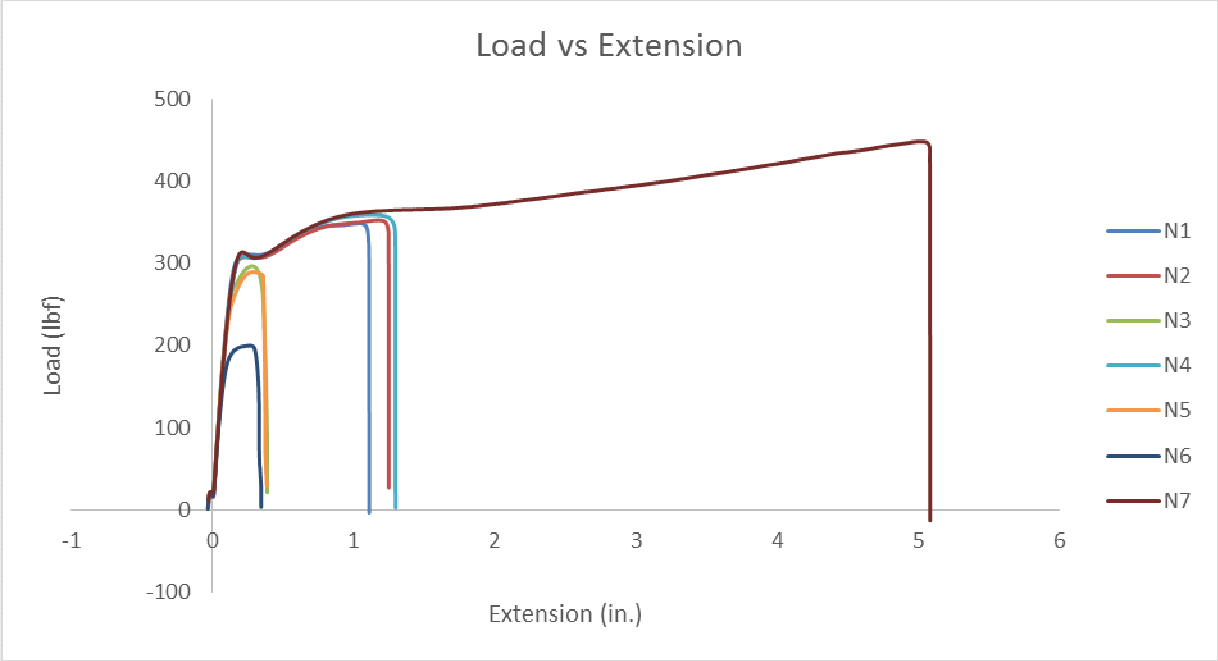

Fig. 19 Load vs Extension curves for tested specimens

Specimen no.	Peak load(lbf)	Modulus(ksi)	% elongation
N1	448.27	147.79	135.54
N2	200.07	145.18	9.18
N3	296.75	158.96	10.34
N4	289.55	154.32	10.26
N5	348.90	153.30	29.61
N6	352.72	150.84	33.308
N7	359.01	147.36	34.59

Table 2. Results from ASTM D638 Tensile testing of PA 11

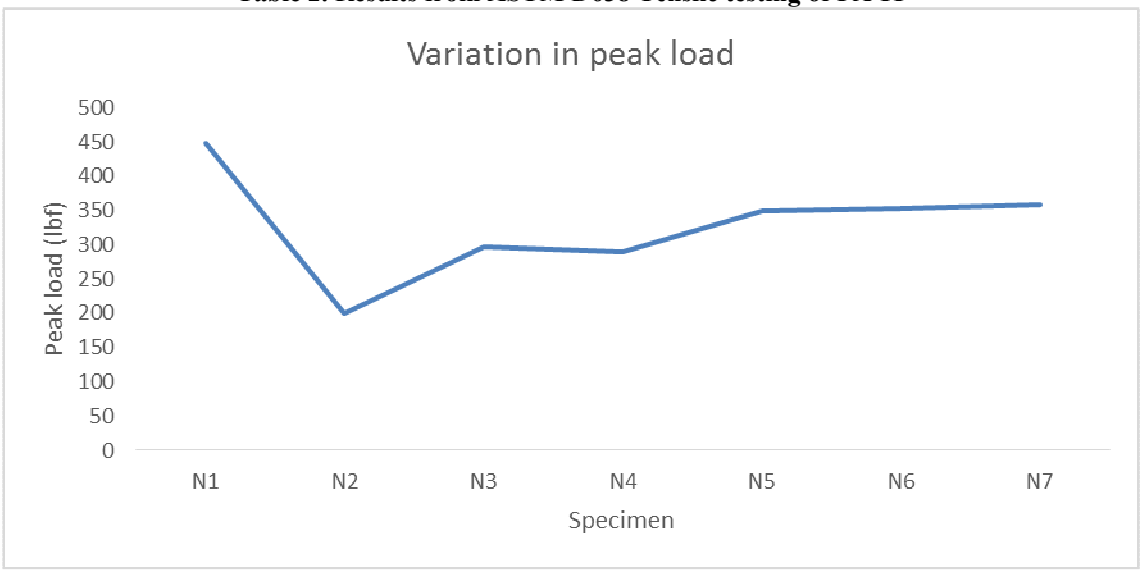

Fig. 20 Variation of Peak load for tested specimens

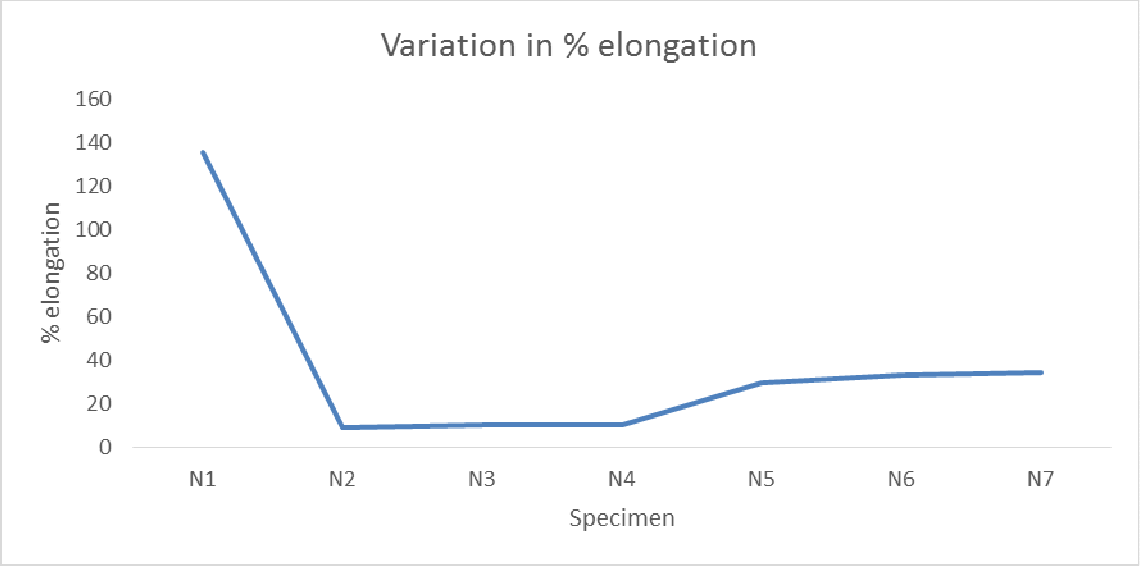

Fig. 21 Variation of % elongation for tested specimens

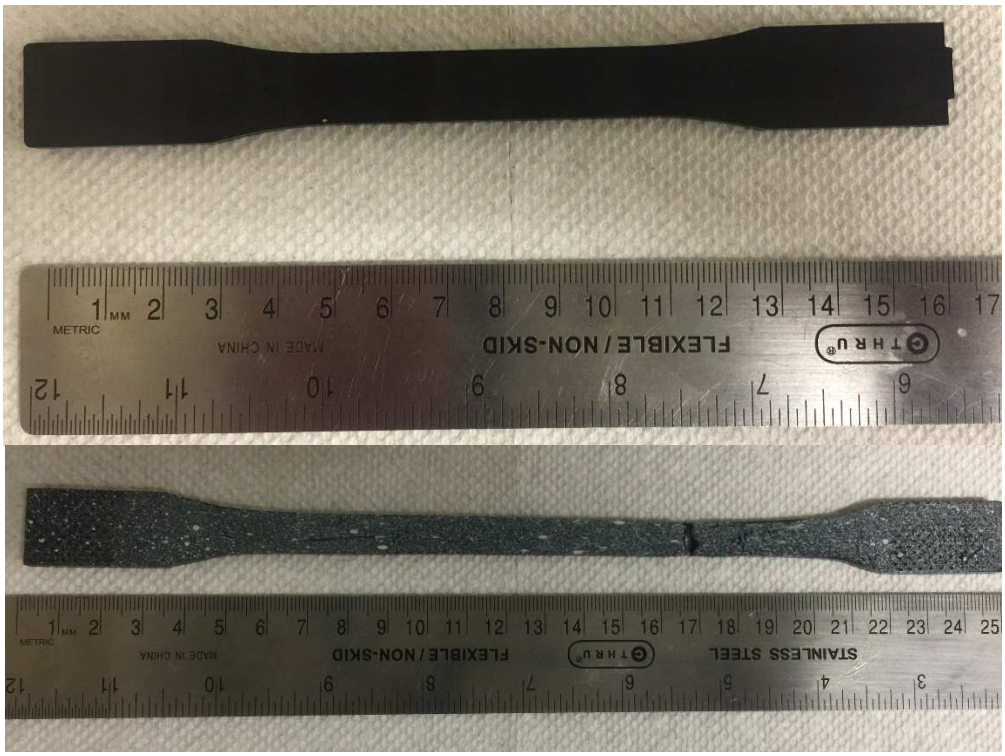

Fig. 22 Scale of elongation of specimen without impingement

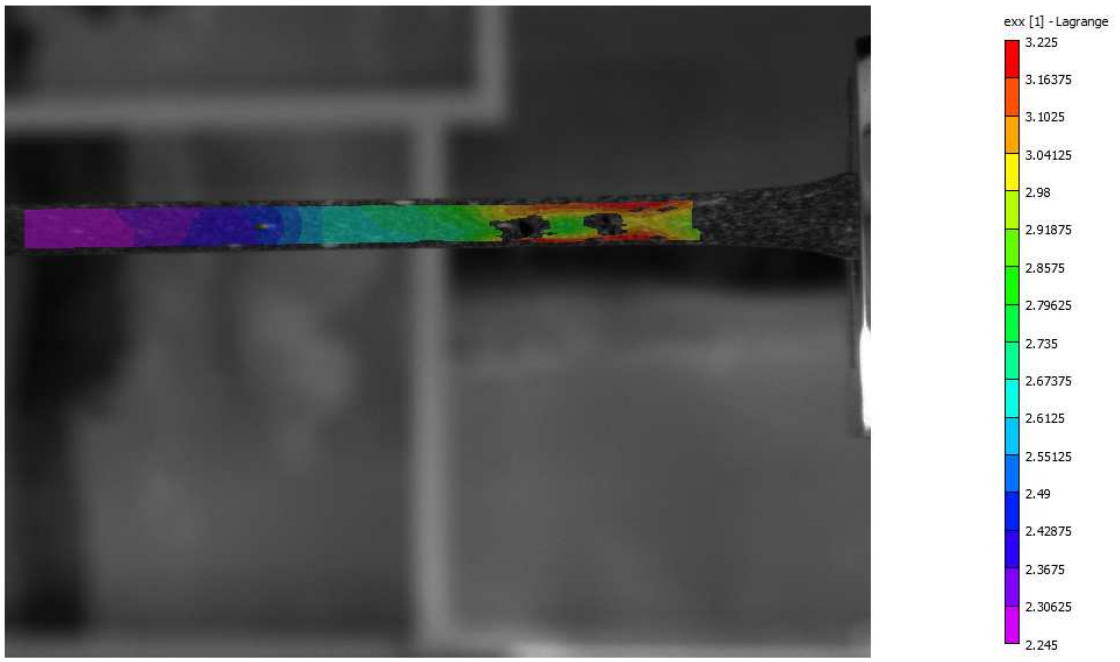

a) N1: (Max strain 3.225)

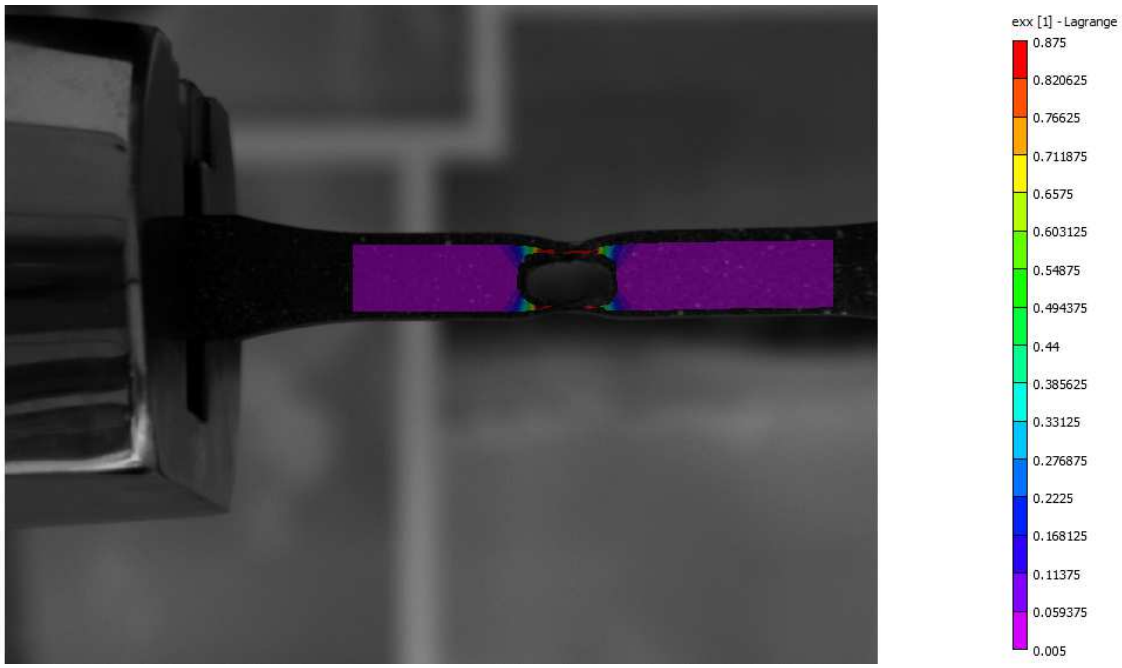

b) N2: (Max strain 0.875)

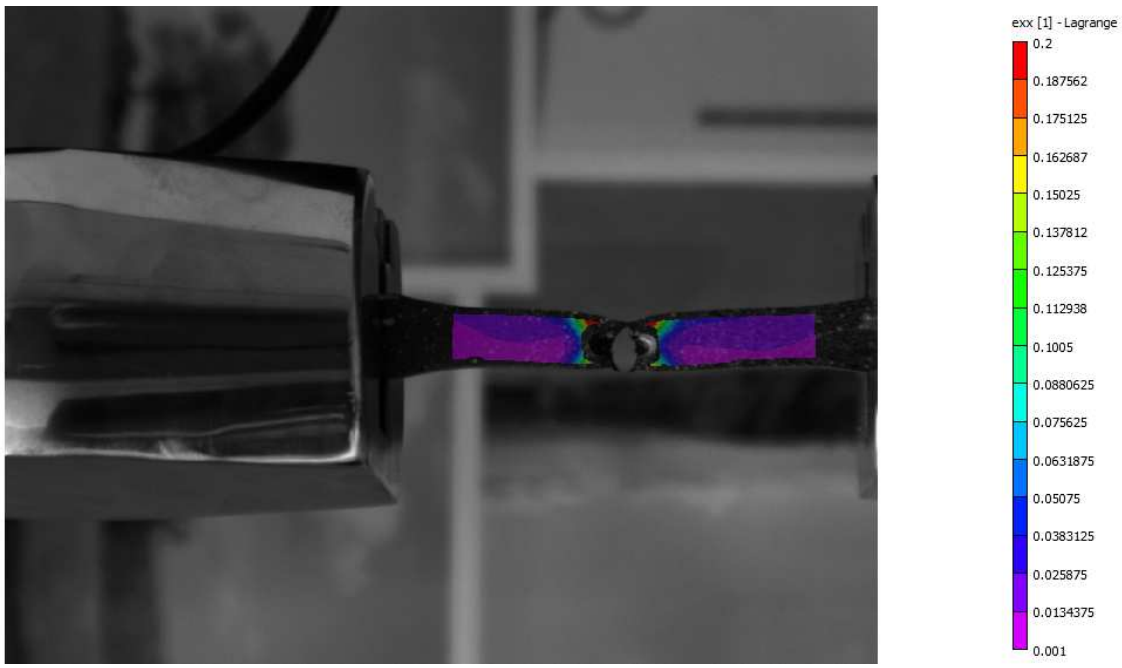

c) N3: (Max strain 0.20)

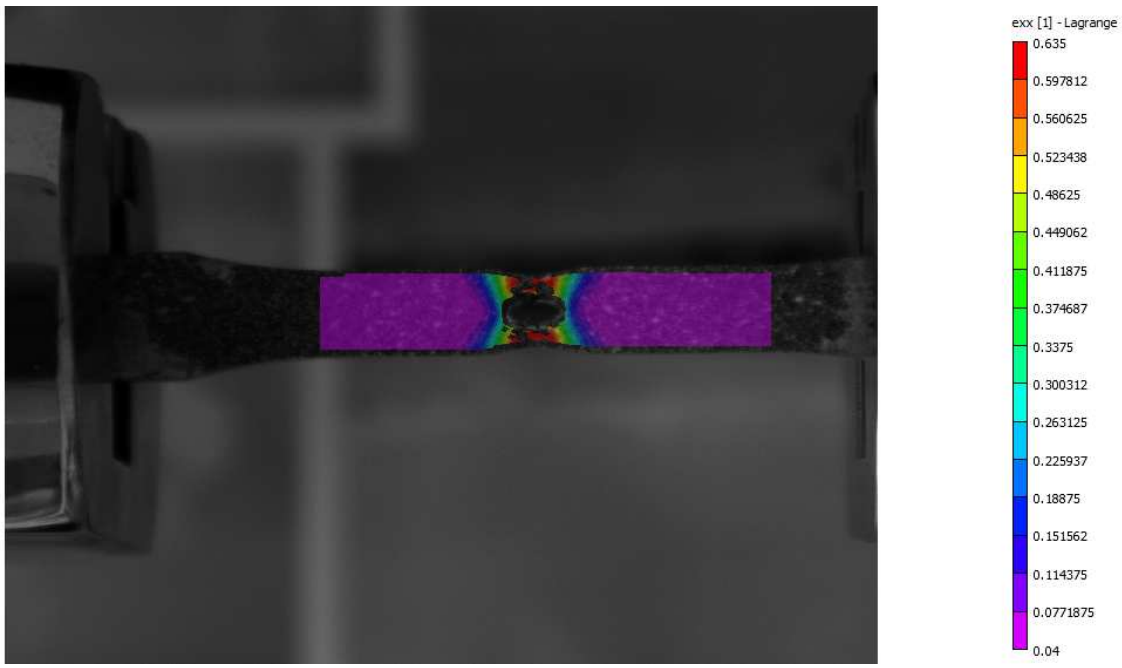

d) N4: (Max strain 0.635)

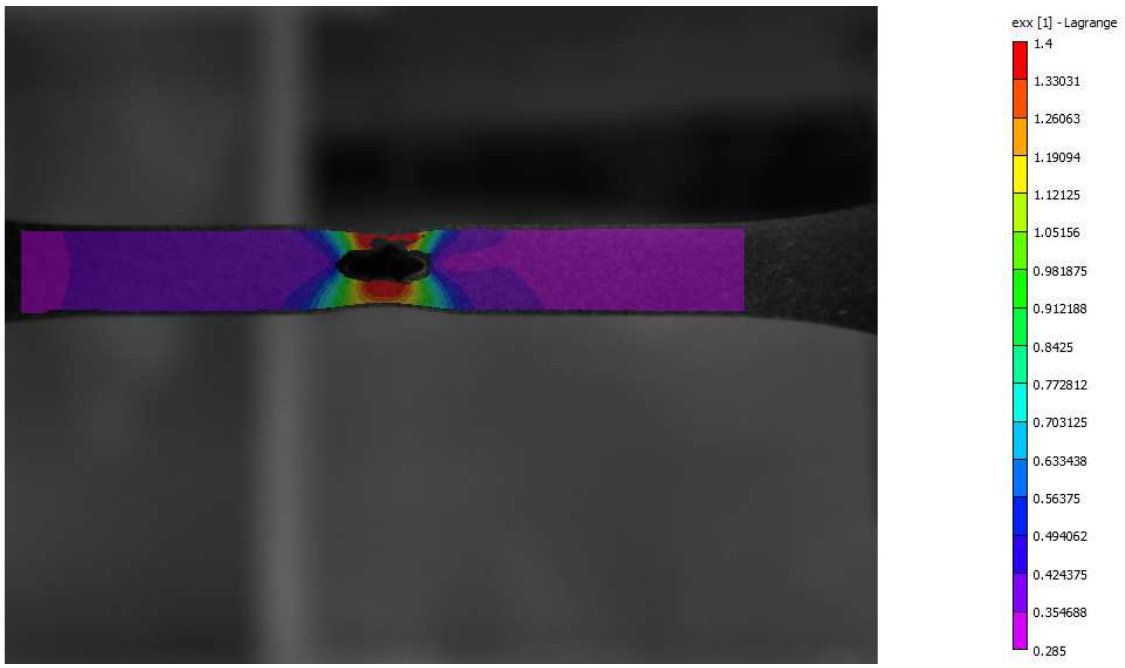

e) N5: (Max strain 1.4)

Fig. 23 Stain maps from DIC

5.1 Effect of impingement on the mechanical properties.

Based on the results obtained, it is evident that any impingement on PA 11 material affects the strength and toughness of the material. The specimen without any impingement has the highest strength and toughness. Impingement has a direct impact on load bearing and ductility of the material. There is a reduction of over 50% in the peak load of the specimen with highest degree of impingement in terms of its size and depth. Similar trend can be observed in the ductility (% elongation) of the material wherein, there is a minimal elongation of impinged specimen. The graphs shown in Fig 19 and Fig 20 clearly indicate the trends for all the tested specimens. Moreover, the DIC strain maps also points out that maximum strain at fracture for specimen with highest degree of impingement is 0.2 when compared with specimen without impingement with a stain of 3.2 at failure.

6.0 FUTURE WORK

- The parameters will be tuned further to match the experimental data.
- Numerical solution will be matched with experimental results.
- The results obtained from simulation are to be verified.
- Simulation of impingement effects on ABAQUS with data obtained experimentally.

6.0 REFERENCES8

[1] A. S. M. International and S. Lampman, Characterization and Failure Analysis of Plastics. ASM International, 2003.

[2] J. R. Davis, Tensile Testing, 2nd Edition. ASM International, 2004.

[3] X. Q. Shi, Z. P. Wang, H. L. J. Pang, and X. R. Zhang, “Investigation of effect of temperature and strain rate on mechanical properties of underfill material by use of microtensile specimens,” Polym. Test., vol. 21, no. 6, pp. 725–733, 2002.

[4] M. B. Saeed and M.-S. Zhan, “Effects of monomer structure and imidization degree on mechanical properties and viscoelastic behavior of thermoplastic polyimide films,” Eur. Polym. J., vol. 42, no. 8, pp. 1844–1854, Aug. 2006.

[5] J. M. L. Reis, L. J. Pacheco, and H. S. da Costa Mattos, “Tensile behavior of post-consumer recycled high-density polyethylene at different strain rates,” Polym. Test., vol. 32, no. 2, pp. 338–342, Apr. 2013.
[6] D. A. Şerban, G. Weber, L. Marşavina, V. V. Silberschmidt, and W. Hufenbach, “Tensile properties of semi-crystalline thermoplastic polymers: Effects of temperature and strain rates,” Polym. Test., vol. 32, no. 2, pp. 413–425, Apr. 2013.
[7] M. R. Petersen, A. Chen, M. Roll, S. J. Jung, and M. Yossef, “Mechanical properties of fire-retardant glass fiber-reinforced polymer materials with Aluminum Tri-hydrate filler,” Compos. Part B Eng.
[8] K. Dyamenahalli, A. Famili, and R. Shandas, “3 - Characterization of shape-memory polymers for biomedical applications,” in Shape Memory Polymers for Biomedical Applications, L. Yahia, Ed. Woodhead Publishing, 2015, pp. 35–63.
[9] A. Awal, M. Rana, and M. Sain, “Thermorheological and mechanical properties of cellulose reinforced PLA bio-composites,” Mech. Mater., vol. 80, Part A, pp. 87–95, Jan. 2015.
[10] A. El Mourid, R. Ganesan, M. Brochu, T. Crochon, and M. Lévesque, “Anisotropic oxidation due to aging in a triaxially braided composite and its influence on tensile failure,” Compos. Part B Eng., vol. 76, pp. 1–12, Jul. 2015.
[11] N. Sadeghian and M. K. Besharati Givi, “Experimental optimization of the mechanical properties of friction stir welded Acrylonitrile Butadiene Styrene sheets,” Mater. Des., vol. 67, pp. 145–153, Feb. 2015.
[12] S. Castagnet, J.-C. Grandidier, M. Comyn, and G. Benoît, “Hydrogen influence on the tensile properties of mono and multi-layer polymers for gas distribution,” Int. J. Hydrog. Energy, vol. 35, no. 14, pp. 7633–7640, Jul. 2010.
[13] A. Kaymakci and N. Ayrilmis, “Investigation of correlation between Brinell hardness and tensile strength of wood plastic composites,” Compos. Part B Eng., vol. 58, pp. 582–585, Mar. 2014.
[14] S. Negi, S. Dhiman, and R. K. Sharma, “Determining the effect of sintering conditions on mechanical properties of laser sintered glass filled polyamide parts using RSM,” Measurement, vol. 68, pp. 205–218, May 2015.
[15] A. R. Torrado, C. M. Shemelya, J. D. English, Y. Lin, R. B. Wicker, and D. A. Roberson, “Characterizing the effect of additives to ABS on the mechanical property anisotropy of specimens fabricated by material extrusion 3D printing,” Addit. Manuf., vol. 6, pp. 16–29, Apr. 2015.
[16] A. Salazar, A. Rico, J. Rodríguez, J. Segurado Escudero, R. Seltzer, and F. Martin de la Escalera Cutillas, “Monotonic loading and fatigue response of a bio-based polyamide PA11 and a petrol-based polyamide PA12 manufactured by selective laser sintering,” Eur. Polym. J., vol. 59, pp. 36–45, Oct. 2014.
[17] M. Kashfuddoja, R. G. R. Prasath, and M. Ramji, “Study on experimental characterization of carbon fiber reinforced polymer panel using digital image correlation: A sensitivity analysis,” Opt. Lasers Eng., vol. 62, pp. 17–30, Nov. 2014.
[18] A. George, H. D. Ngo, and A. Bellare, “Influence of crystallization conditions on the tensile properties of radiation crosslinked, vitamin E stabilized UHMWPE,” J. Mech. Behav. Biomed. Mater., vol. 40, pp. 406–412, Dec. 2014.
[19] D. B. Knorr Jr., K. A. Masser, R. M. Elder, T. W. Sirk, M. D. Hindenlang, J. H. Yu, A. D. Richardson, S. E. Boyd, W. A. Spurgeon, and J. L. Lenhart, “Overcoming the structural versus energy dissipation trade-off in highly crosslinked polymer networks: Ultrahigh strain rate response in polydicyclopentadiene,” Compos. Sci. Technol., vol. 114, pp. 17–25, Jun. 2015.

.

Description of any Problems/Challenges

The project progress is satisfactory according to the schedule of tasks table. Good communications between the PIs, students and program director is well maintained. There are a few technical challenges identified and will be addressed in the future quarters, which is listed as follow:

PA samples acquistion from industrial parterner:
PA materials samples have been received from the industrial patterned. Testing plans are current been discussed between CU Denver and ASU. Preliminary imaging and testing results are presented in this quarterly report. PE tensile bars will be ordered from industrial vendor.

(c) Planned Activities for the Next Quarter

Besides the planned activities mentioned in section (b), here are the future work for the next quarter:

FEKO and EFG simulation for PE and PA damage with experimental validation: A systematic study and imaging will be conducted in Q4. Experimental results will be analyzed and also validated by the simulation results. Raw data will also be delivered to ASU for further analysis.

XFEM simulation with multiphsics damage coupling: Following the previous kick offmeeting and phoen discussions, it was identified that other environmental damage may contribute to the final failure of pipeline systems, such as diffusion. ASU team is working on a general methodology to include this type of damage in the current simulation framework,